Numerical study of the exposure to volatile organic compounds (VOCs) released from liquid crystal displays in an office

Cunteng Wang, Jingcui Xu, Yunxi Huo, Hai Guo*

Indoor Air and Aerosol Science Laboratory, Department of Civil and Environmental Engineering, The Hong Kong Polytechnic University, Hong Kong, China

* Corresponding author (s)

Hai Guo, Department of Civil and Environmental Engineering, The Hong Kong Polytechnic University, Hung Hom, Hong Kong. Email: hai.guo@polyu.edu.hk

Abstract

People spend about 90% of their time indoors and indoor volatile organic compounds (VOCs) are critical to human health. Liquid crystal displays (LCDs) widely used in offices are a new source of indoor VOCs, with an emission rate of 8.25×10^9 molecules·s^{-1}·cm^{-2} reported by Liu and Abbatt (2021). Therefore, this work studied the exposure to LCD VOCs in a four-person office environment through numerical simulation. Air change rate per hour (ACH), geometric setting and partition were also investigated. The results revealed that at an ACH of 4, human users inhaled 0.07%-0.25% of the released VOCs. The deviations for different users were 4-9 times due to various locations. Different geometric settings resulted in 2-3 times exposure deviations. Increasing the ACH to 20 led to an 88% reduction. The estimated lifetime exposure via inhalation was 8.2×10^{18} VOC molecules, or 1 mg per LCD. This study contributed to the understanding of exposure to VOCs from LCDs.

Keywords: VOC, Ventilation, Exposure, LCD, Indoor contaminant

Introduction

People spend 90% of their time indoors, and indoor air quality is of great importance for human health because of exposure to indoor air contaminants.[1-3] Volatile organic compounds (VOCs) are one of the major indoor contaminants and have attracted extensive research interest due to their adverse health effects.[4-8] Long-time exposure to VOCs can cause discomfort, inflammation of respiratory tract, heart disease and even cancer.[9-11] Therefore, studying human exposure to indoor VOCs is crucial to evaluate health effects and develop control measures to improve indoor air quality.

Indoor substances and human activities are the major sources of indoor VOCs.[12, 13] Many studies have characterized different types of indoor VOC sources, such as building materials,[14] decorations,[15] personal care products,[16] fragrance products[17] and human activities (cleaning, cooking and display).[18, 19] Apart from these traditional sources, electronic products may also release chemicals and become a source of indoor VOCs. Recently, Liu and Abbatt [20] pinpointed that liquid crystal displays (LCDs) are an important source of indoor VOCs and described the emission strength of VOCs from LCDs. They found that the emission strength was as high as 8.25 $\times 10^9$ molecules/($s \cdot cm^2$). The annual product of LCDs continues to increase, and the production of LCD monitors in 2018 was with 198 million square metres.[21, 22] However, exposure of human users to VOCs from LCDs in indoor environments has not been sufficiently studied and therefore remains unclear, though it is an essential component of electronic devices that thrive in modern offices.

A handful of studies have been conducted on the dispersion and exposure of VOCs in industry or outdoor environments. Chang et al. [23] and Chang et al. [24] studied the exposure of thin film transistor LCD workers to VOCs in the workplace and evaluated the health effects, including

hypertension and kidney dysfunction. VOC samples were collected using canisters and analyzed by gas chromatography - mass spectrometry. The results showed that LCD workers exposed to high levels of VOCs were associated with elevated blood pressure. Wang et al. [25] evaluated the long-term exposure of workers in the thin film transistor LCD industry to multiple chemicals. During different work shifts, the concentrations of surrogates of ethanol, acetone and propylene glycol monomethyl ether acetate were as high as 2480 ppb, 624 ppb and 2241 ppb, respectively. Fu et al. [26] numerically studied the NO_x-O_3 photochemical cycle and the air pollutants reactive dispersion around an isolated building from point sources of roof and ground. The distribution of air pollutant indicated a self-similar and stratified pattern, contributing to the natural deposition.

Regarding the indoor VOCs, Yang et al. [27] studied the removal effect of different ventilation types on VOCs released from a surface source. They found that the VOC concentrations generated by a grille diffuser were lower than those of displacement and square diffusers. Deng and Kim [28] carried out numerical simulations to study the concentrations of VOCs released from a new carpet in a residential building, and pointed out the importance of ventilation in removing VOCs. Zhang et al. [29] simulated TVOC pollutants from a new floor at different supply rates of fresh air under re-circulated ventilation, and found uneven distribution in various zones. Tong and Liu [30] simulated the distribution of VOCs released from cabin decorations under solar radiation and found that solar radiation affected temperature distribution and VOC distribution. Zhao et al. [31] studied the TVOC concentration and dilution in an enclosed train compartment by numerical methods and discovered that airflow was vital to the pollution level and TVOC distribution, and that TVOC distribution was non-uniform. These studies mainly focused on traditional VOC sources in indoor environments, including floors, carpets and decorations. They also indicated that the distribution of VOCs in indoor environments was reliably captured by numerical simulations

of computational fluid dynamics (CFD). However, as a new source in indoor environments, the exposure of VOCs emitted from LCDs are still lacking.

Human exposure to VOCs depends on the emission strength and airflow pattern in indoor environments. The latter determines the distribution of VOC molecules and the removal efficiency of ventilation. Many indoor parameters affect the airflow pattern and the exposure of VOC molecules. For example, human users have different preferences for the geometric setup of their offices, including the orientation and direction of their desks. As a result, the relative positions of the users to the ventilation diffusers could vary, which could affect the exposure of VOC molecules. Partition is a common part of desks and affects the airflow patterns,[32-34] thereby affecting the exposure of VOCs. In addition, air change rate per hour (ACH) is important in characterizing ventilation rate, and ASHRAE specifies that the ACH for offices should be between 2 and 4.[35] Many studies suggest increasing ACH to reduce airborne particle concentrations and indoor contaminants.[36, 37] The ACHs for different building environments are much higher, especially after the COVID-19 pandemic. The impact of these indoor parameters on indoor VOC exposure has not yet been resolved, which can help in designing appropriate interventions.

In this study, we evaluated inhalation exposure of human users to VOCs released from LCDs in an office. This study aimed to investigate the inhaled fraction of VOCs to the emission from the LCDs, i.e., intake fraction. Then, the impacts of the work-station setups, physical desk-based partitions, users at different positions of the office, and ACH on the exposure were systematically investigated. Finally, the lifetime exposure to VOCs via inhalation was evaluated based on the intake fraction, emission strength, and exposure duration.

Methodology

Geometric setting of an office

A four-person office on campus was examined to study the inhalation exposure of occupants to VOC molecules from LCDs in indoor environments. The length, width and height of the office were 3.8 × 4.2 × 2.8 m, as shown in Figure 1. The office included a load-bearing column, a cabinet, four tables, monitors and human users. It also had two inlet diffusers and two outlets. The inlet diffuser had four separate inlets that supplied fresh conditioned air at an angle of 45 degrees to the roof. The length and width of the inlet diffuser and outlet were both 0.94 × 0.44 m, as shown in Figure 1b. The length, width and height of the desk were 1.25 × 0.7 × 0.7 m. The height of the partition was 0.78 m, and the thickness was 0.03 m. Actual airflow velocity from the typical air conditioning diffuser was measured in an office on the university campus. The air conditioner controller had three positions and could adjust the airflow to a maximum velocity of 1 m/s with a temperature of 20°C (Air Velocity Meters VELOCICALC TSI 9535). Therefore, in this study, the different inlet velocities of 0.1 m/s, 0.2 m/s, 0.5 m/s, 0.7 m/s and 1.0 m/s were investigated, which corresponded to the air change rate per hour (ACH) of 4, 8, 20, 28 and 40, respectively. Typically, ASHRAE Standard 62.1-2022 specifies an ACH of 2-4 for offices.[35] In many buildings, ACH can be adjusted to have a higher value. This study investigated the exposure of occupants to VOCs in an office with a much higher ACH of up to 40.

The skin area of human occupants in this study was 1.6 m^2, in the range of 1.6 - 2.0 m^2 for adults, as indicated by a study.[38] For moderate office work, the heat flux was set as 39 W/m^2 and the heat dissipation as 62.4 W, in the range given by the ASHRAE handbook for heating, ventilating and air-conditioning (HVAC) applications.[35] The mouth of a human occupant was set to be a circle with a diameter of 1.4 cm, matching the area of 0.7 - 1.7 cm^2 of the human mouth.[39]

The suction flow rate was set to 0.84 m^3/h, the mean airflow rate of inhaled air.[39] The moderate heat transfer through glass windows was set to be 12.8 W/m^2, as suggested by a previous study.[40] The glass window was set to be closed in the simulation.

Depending on the preferences of human users, offices may have different settings. Therefore, in this study, four different office geometric settings were created for the investigation. For setting 1, desks were set up facing each other along the glass and side walls (Figure 1a and 1c). For setting 2, desks were placed side by side along the glass and side walls (Figure 1d). For setting 3, desks were placed side by side along the glass and back wall (Figure 1e). For setting 4, desks were set side by side along the two side walls (Figure 1f). In total, five ACHs, four geometric settings, and two partition settings were studied for 40 cases. Detailed research cases and boundary conditions are shown in Tables 1 and 2.

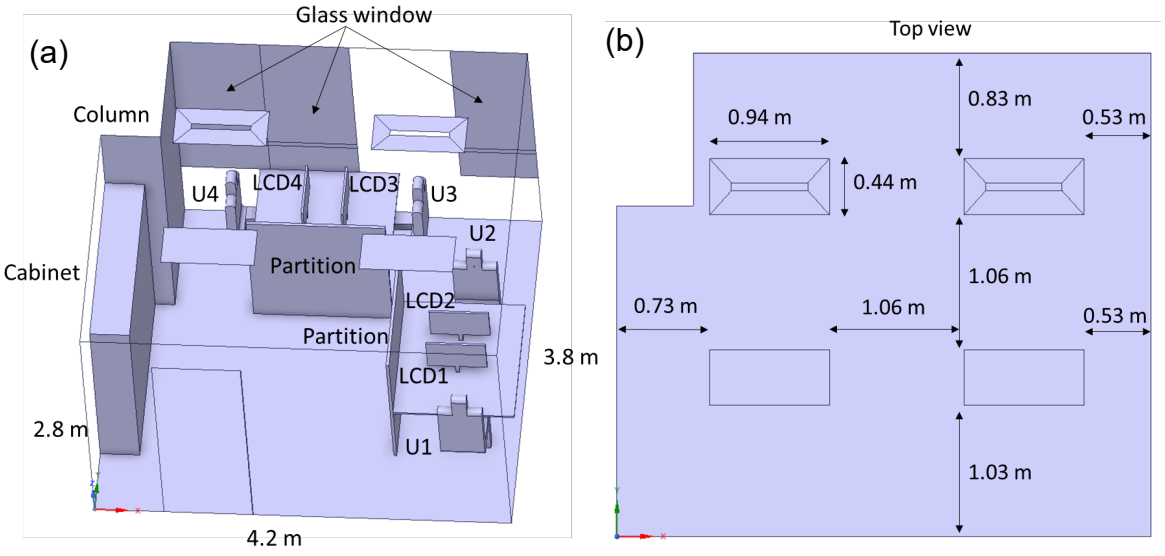

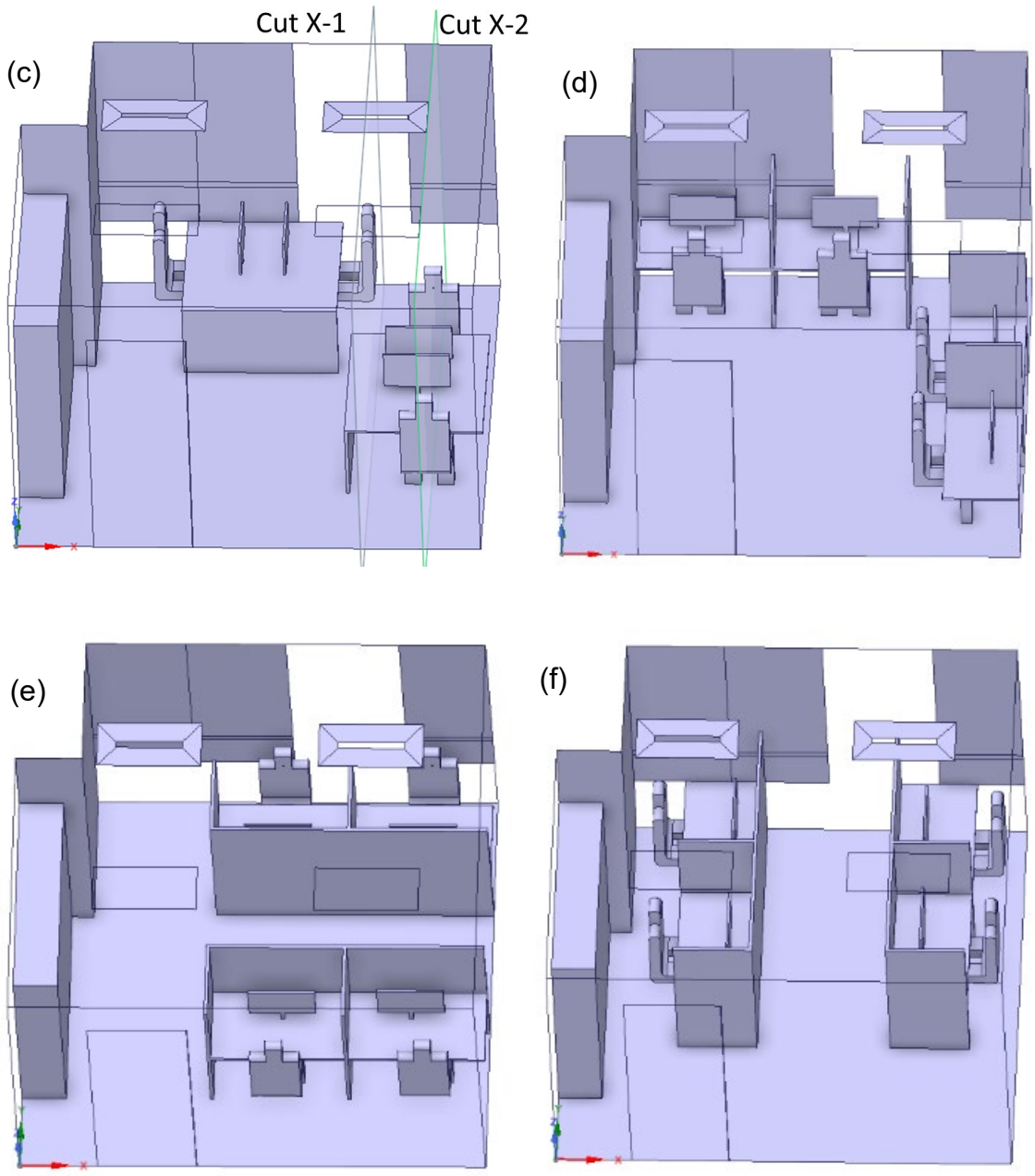

Figure 1. Geometric settings of the office in this study. (a) Setting 1 with partition, (b) Setting 1 with top view, (c) Setting 1 without partition, (d) Setting 2 with partition, (e) Setting 3 with partition, (f) Setting 4 with partition. The cuts X-1 and X-2 were used to show the airflow fields.

Table 1. Parameters studied in this work

Parameter	Value
Geometric setting of desks	1, 2, 3, 4
Workstation partition	With and no partition
Air change rate per hour (ACH)	4, 8, 20, 28, 40
Human occupants in office	1, 2, 3, 4
VOCs source	Monitor 1, 2, 3, 4

Table 2. Boundary conditions for numerical simulations

Item	Condition
Inlet diffusers	T = 20°C, V = 0.1, 0.2, 0.5, 0.7, 1.0 m/s for ACHs of 4, 8, 20, 28, 40, respectively Four parts oriented at 45° to the roof
Outlet	Pressure outlet
Walls, desks, roof, ground, door	Reflective, isothermal inner walls, no slip
Glass, windows	Heat flux: 12.8 W/m^2, no slip
Human users	Oral inhalation flow rate: 0.84 m^3/h Heat flux: 39 W/m^2 Skin surface: 1.6 m^2 no slip Capture of VOC molecules
LCD screen	Heat flux: 12.5 W/m^2; area: 0.22 m^2; VOC source

Numerical modelling, meshing and validation

Ansys Fluent was employed to simulate VOC dispersion and exposure of occupants in the office.[27, 31] The airflow field in the office was obtained using Eulerian and Lagrangian methods. The RNG k-Ɛ model with enhanced wall treatment was used to solve the Navier-Stokes equations for the continuous phase.[40-43] A stable simulation of the continuous air phase was performed as the airflow in the office was stable. The carbon dioxide particle in the discrete phase model (DPM) was employed to track the VOC phase transportation. As indicated in previous studies, the gaseous phase (e.g., SF_6 and CO_2) had diffusion features similar to the particles and was widely used to represent the particle phase in indoor environments.[44-47] The dispersion of the particle phase in this work was also validated by comparing it with the experimental gaseous contaminant diffusion (SF_6),[48] which can be seen in the following validation part. Using the carbon dioxide particle to simulate the VOC molecule diffusion, the inhalation exposure can be directly obtained from the numerical simulations via simulating the inhaling airflow. In addition, the realistic inhalation exposure can be simulated by considering the complex airflow from the inhalation process and the thermal plume near the inhalation zone.

The random walk model was employed to consider the effect of turbulence on particle transport.[41] To consider the airflow caused by the heated bodies, the air density was set using the Boussinesq setting, which integrated the density change caused by the temperature difference and was applicable for the small indoor temperature difference. [40, 49] The thermal expansion coefficient was set to 0.003344 K^{-1}, which is the reciprocal of indoor operating temperature. [49] Pressure-velocity coupling with the SIMPLE scheme was used for solution calculation. The second-order method was used to discretize pressure, momentum, turbulent kinetic energy, turbulent dissipation rate and energy. The residuals of 10^{-3} were used for velocities, continuity, k and epsilon convergence, and the 10^{-6} residuals were used for energy convergence. The Reynolds-averaged

Navier-Stokes (RANS) equations were written as following Equations (1) – (3) for the RNG k-Ɛ model:

$$\frac{\partial \rho}{\partial t} + \nabla \cdot (\rho U) = 0 \tag{1}$$

$$\frac{\partial (\rho \vec{U})}{\partial t} + \nabla \cdot (\rho \vec{U} \otimes \vec{U}) = -\nabla p + \nabla \cdot (\mu \nabla \vec{U} - \overrightarrow{u_i' u_j'}) + \rho [g \beta_T (T - T_0)] \overrightarrow{e_3} \tag{2}$$

$$\frac{\partial (\rho C_p T)}{\partial t} + \nabla \cdot (\rho C_p T \vec{U}) = \nabla (\lambda \nabla T - \rho C_p \overrightarrow{u_i' T'}) \tag{3}$$

where ρ is air density, U is time-average velocity, p is static pressure, u_i' is fluctuating velocity, g is gravitational acceleration, β_T is temperature coefficient, $\overrightarrow{e_3}$ is the direction of the buoyancy force, C_p is specific heat capacity, T is air temperature, $\rho \overline{u_i' u_j'}$ and $\rho \overline{u_i' T'}$ are the average Reynolds-stress tensor and turbulent heat flux, respectively. They are modelled by Equations (4) and (5) as follows:

$$\rho \overline{u_i' u_j'} = -\mu_T S_{ij} + \frac{2}{3} \rho k \delta_{ij} \tag{4}$$

$$\rho \overline{u_i' T'} = -\alpha_t \nabla T \tag{5}$$

where $k = \frac{\overline{u_i' u_i'}}{2}$ is the turbulent kinetic energy, δ_{ij} is the Kronecker tensor, α_t is the turbulent thermal diffusivity, and $\mu_T = \frac{C_\mu \rho k^2}{\varepsilon}$ is the eddy viscosity, ε is the turbulent dissipation rate, S_{ij} is shear strain rate tensor. The transport equations of turbulent kinetic energy and dissipation rate are written as Equations (6) and (7):

$$\frac{\partial (\rho k)}{\partial t} + \nabla \cdot (\rho k \vec{U}) = \nabla \left[\left(\mu + \left(\frac{\mu_t}{\sigma_k} \right) \nabla k \right) \right] + G_s + G_t + \rho \varepsilon \tag{6}$$

$$\frac{\partial(\rho\varepsilon)}{\partial t} + \nabla \cdot \left(\rho\varepsilon\vec{U}\right) = \nabla\left[\left(\mu + \left(\frac{\mu_t}{\sigma_\varepsilon}\right)\nabla\varepsilon\right)\right] + C_1(G_s + G_t)\left(1 + C_2R_f\right)\frac{\varepsilon}{k} - C_3\frac{\rho\varepsilon^2}{k} \qquad (7)$$

where $G_s = \mu_t S_{ij}\nabla \cdot \vec{U}$, $G_t = g_i\beta_T\left(\frac{\mu_t}{Pr_t}\right)\nabla T$, $R_f = -\frac{G_t}{G_t+G_s}$, $S_{ij} = \frac{\partial\overline{u_i}}{\partial x_j} + \frac{\partial\overline{u_j}}{\partial x_i}$, $C_1(\eta) = 1.42 - \frac{\eta(1-\eta/4.38)}{1+0.012\eta^3}$, $\eta = k\frac{\sqrt{S_{ij}S_{ij}}}{\varepsilon}$, C_2, C_3, C_μ, σ_k, and σ_ε are the constants in the modelling with values of 0.0, 1.68, 0.085, 0.719 and 0.719, respectively.

Fluent meshing was employed to create a poly-hexcore mesh as shown in Figure 2. A uniform body mesh of size 16 mm was created. The surface mesh for walls, tables, roof and ground was set to 16 mm. The surface mesh for humans was set to 8 mm. The office wall had six inflation layers to capture the flow field near the wall. The last ratio function was employed to transition between the surface mesh and the body mesh. For the enhanced wall function, the y+ of the computational domain surface was approximately one.[40-42] The number of mesh cells for the study case was approximately 14 million.

The mesh independence check was performed by comparing three types of meshes: a coarse mesh of 6.6 million cells, a medium mesh of 14 million cells and a fine mesh of 26 million cells. The coarse mesh had larger body cells, while the fine mesh had finer surface meshes. The area-averaged velocities of the three x, y and z cross sections were compared, as shown in Table 3. The differences between the medium and fine meshes of the three cross sections were 1.2%, 3.7% and 2.5%, respectively, which were less than 5%. In order to balance cost and efficiency, a medium mesh of 14 million was used in this study, as shown in Figure 2.

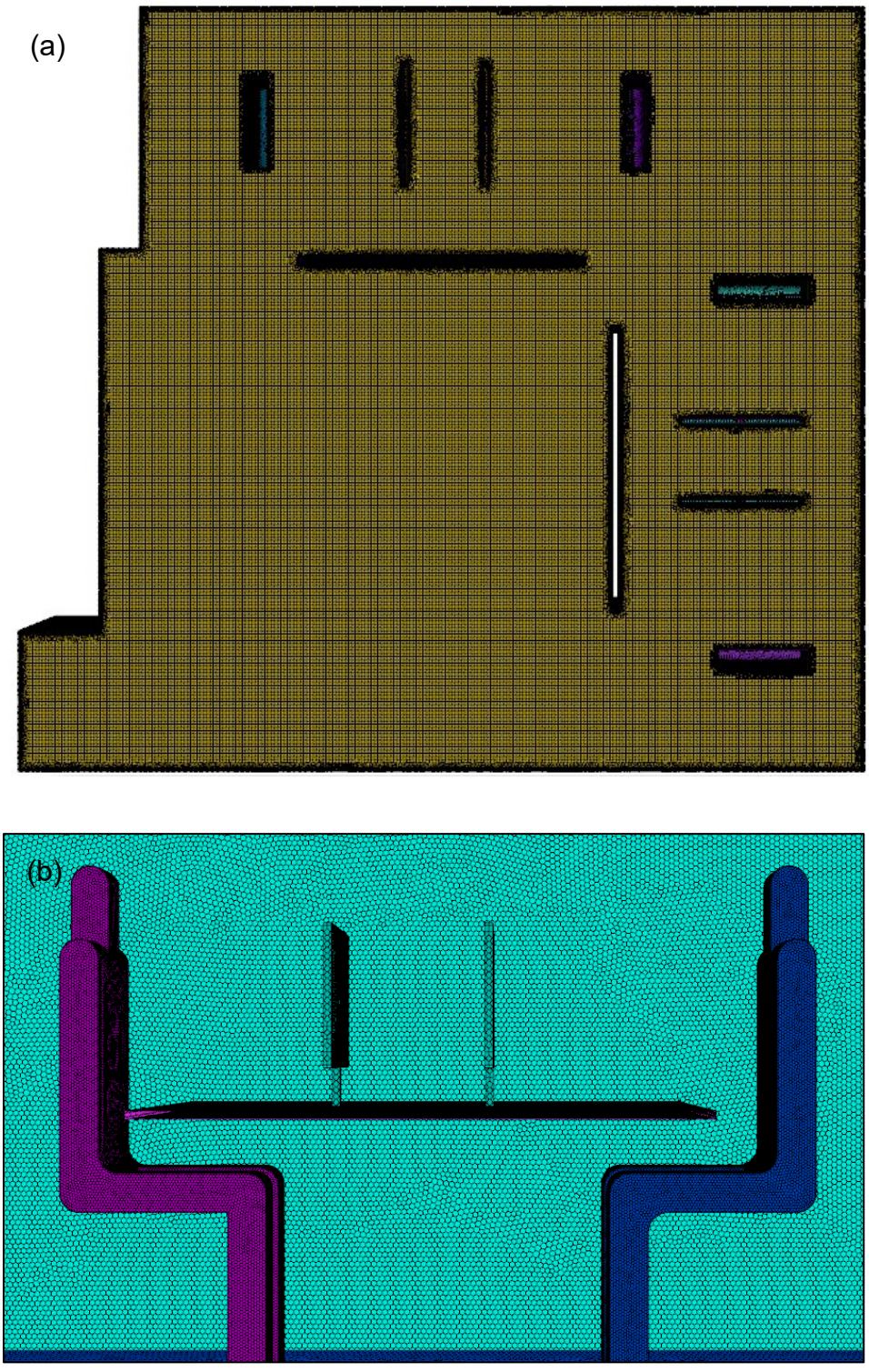

Figure 2. Poly-hexcore mesh for the case of partitioned geometric setup 1. (a) Uniform body mesh and (b) surface mesh of human user 2 and the desk.

Table 3. Independent check of coarse, medium and fine meshes.

Mesh cell number	**6.59 million**	**14.04 million**	**26.04 million**
X cross section	0.2099	0.1948	0.1972
Relative error	-	7.2%	1.2%
Y cross section	0.2027	0.1969	0.1896
Relative error	-	2.9%	3.7%
Z cross section	0.2179	0.2387	0.2327
Relative error	-	9.5%	2.5%

The numerical model was validated by comparing it with the experimental results in reference.[48] The numerical domain for validation was the same as the experiment's geometric setup in reference, as shown in Figure 3. The experimental setup was 6.0 × 3.9 × 2.25 m in length, width and height, comparable to the studied office in this work. The gaseous contaminant was released behind the human occupant and 0.1 m above the floor. The same numerical setup was employed for the validation, including the meshing and solving scheme. In the simulation, the particles were released at the exact location of the experimental source of the gaseous contaminant. The velocity, temperature and particle concentration profiles along four poles in the vertical direction were extracted from the numerical simulation, as shown in Figure 3. The comparison of the simulation and experimental results is shown in Figure 4. The numerical results of the velocity, temperature and concentration profiles agreed reasonably well with the experimental results, indicating the reliability of the numerical model in this study.

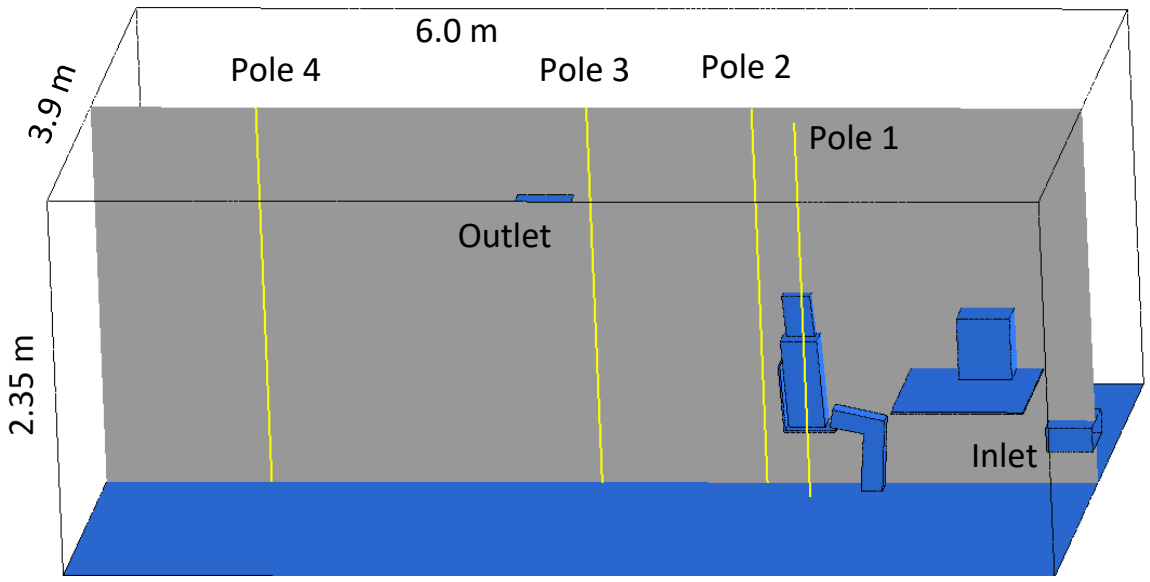

Figure 3. Geometric setup of the experimental setup used to validate the numerical simulations of this work

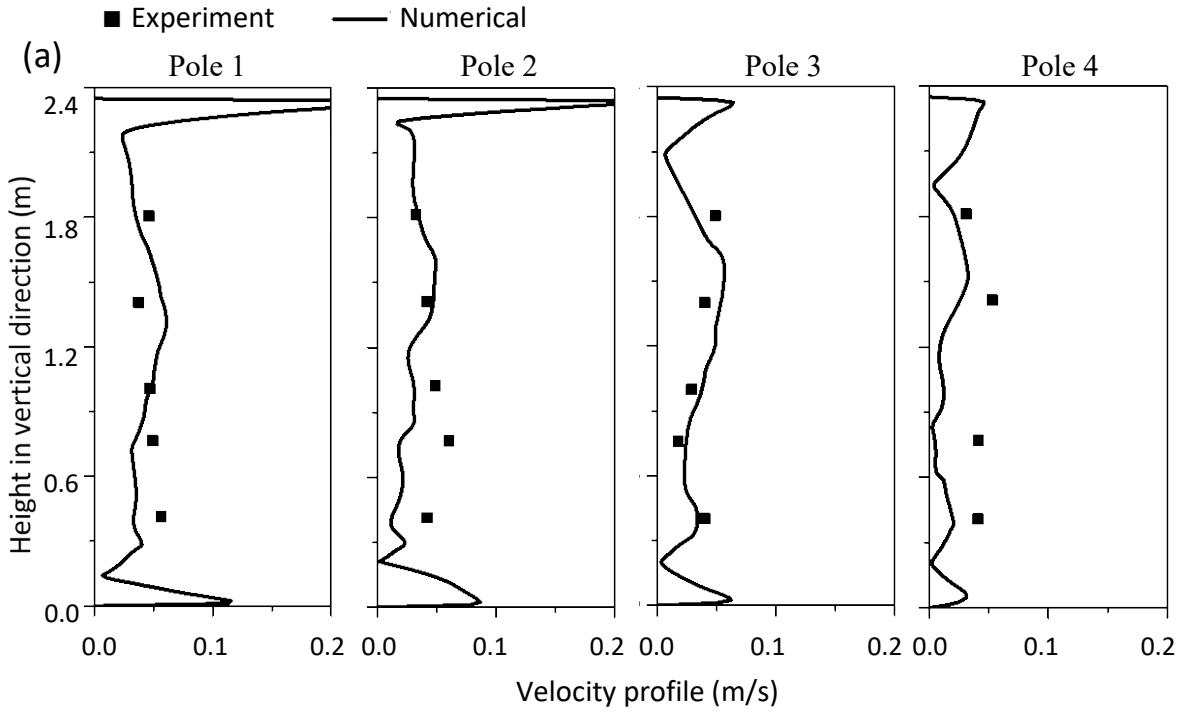

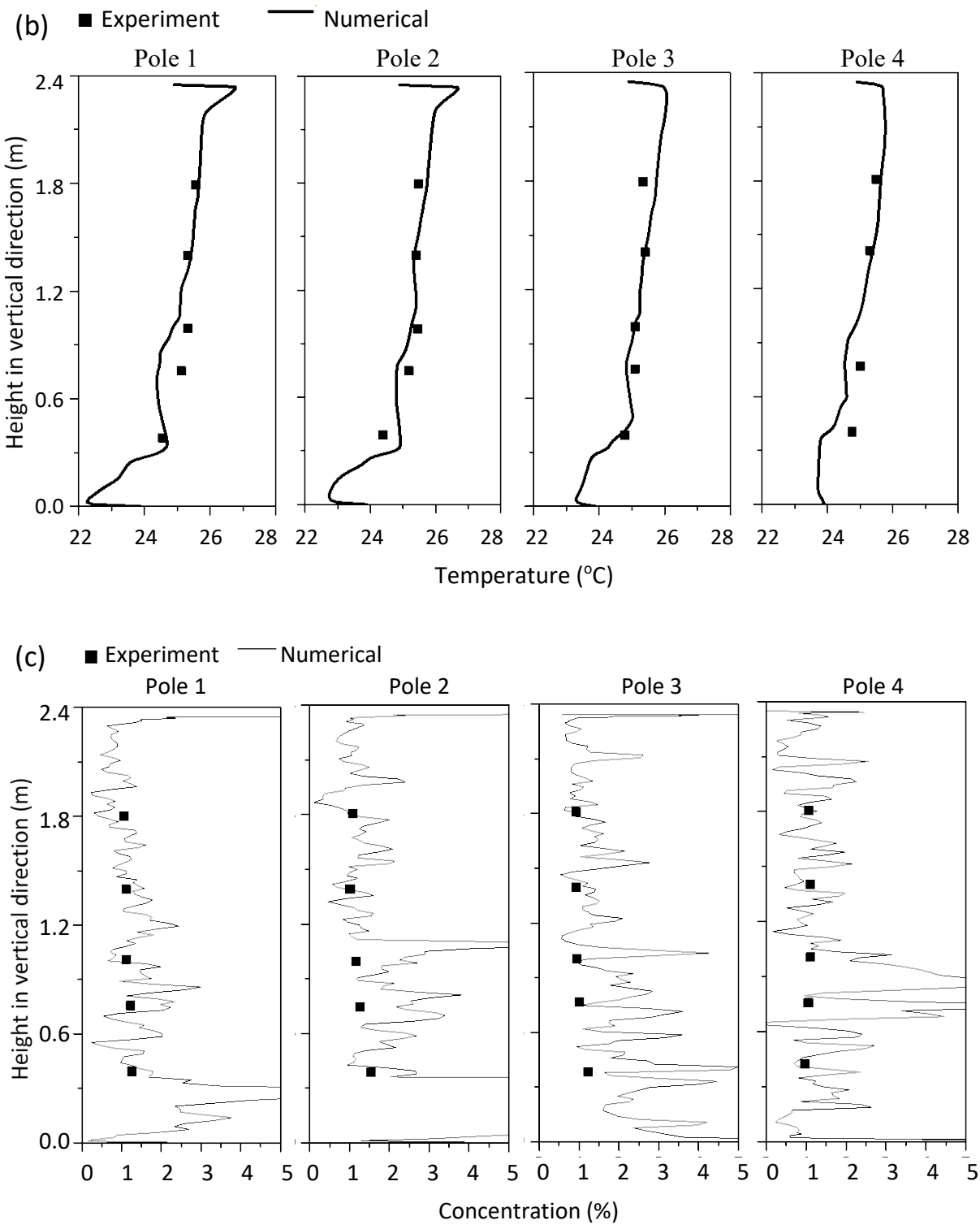

Figure 4. Comparison of experimental and numerical results at four different poles. (a) Velocity profiles, (b) temperature profiles, and (c) concentration profiles.

Evaluation indices of exposure to VOCs

This study evaluated the lifetime exposure dose to LCD VOCs through inhalation, which was based on an average human inhalation flow rate of 0.84 m^3/h.[39] The inhaled fraction (*IF*) of the human users was calculated by Equation (8).

$$\mathrm{IF} = \frac{N_{Inhale}}{N_{Release}} \tag{8}$$

where N_{Inhale} is the number of VOC molecules inhaled by human user and $N_{Release}$ is the number of VOC molecules released from the LCDs. To obtain the intake fraction, 800,000 carbon dioxide particles were released from LCDs to represent the VOC molecules, with 200,000 molecules released from each LCD for stable results [41]. N_{Inhale} was obtained from the numerical simulations of tracking the carbon dioxide particle under various scenarios, i.e., four geometric setups, five ACHs, partitions and four users. The lifetime exposure dose via inhalation (D_{Inhale}) was then calculated by Equation (9).

$$D_{Inhale} = ER \cdot Area \cdot Time \cdot IF \tag{9}$$

where *ER* is the emission rate of LCD VOCs, *Area* is the area of emission source, *Time* is the lifetime of exposure. Liu and Abbatt 2021 [20] revealed that the emission rate from LCD was about 8.25×10^9 molecules/($s \cdot cm^2$). The area of the source in this study was 0.22 m^2 per LCD. The exposure time was assumed to be 30 years, with 8 hours per day. The lifetime mass exposure dose was calculated as given by Equation (10).

$$MD_{Inhale} = \frac{D_{Inhale} \cdot M}{N} \tag{10}$$

where MD_{Inhale} is the mass doses via inhalation; M is the molar mass; N is the amount of substance, which is 6.02×10^{23}. The estimated molecular form of LCD VOC molecules is C_5H_9 [20], with an M value of 69.12 g/mol.

Results

Airflow field and temperature contour in the office

Airflow is important for the dispersion of indoor contaminants. Figure 5 shows the cross sections of airflow fields in the x-axis for the case of geometric setup 1 with an ACH of 4. For the cross-section passing through the inlet diffuser (Figure 5a), the fresh air streams from the diffuser was initially released at an angle of about 45°C to the roof, but then quickly turned downward, and the two air streams from the opposite inlets of the diffuser merged and rushed into the lower part of the office as the mainstream. There were several large vortices in this cross-section. For the cross-section passing through the human occupants (Figure 5b), strong upward thermal plumes was observed arising from two human occupants with a velocity of about 0.5 m/s. The plumes then induced several large vortices in the upper part of the office. The large-scale up-and-down flipping of the air in the office implied well-mixed situation in the office.

Figure 6 shows the airflow fields in the x-axis cross sections for the case of geometric setup 1 with an ACH of 40. For the cross-section passing through the inlet diffuser (Figure 6a), the fresh air streams from the diffuser had enough momentum to move forward, with an initial angle of 45° C to the roof. One air stream moved forward, impacted the wall, and then turned mostly downward to attach to the wall. The other air stream moved forward and impacted the opposite wall but the stream was at a higher position in the office. Therefore, the two opposing streams formed a large loop with an airflow flowing down the wall and a weaker upward flow in the middle area. For the

cross-section passing through the human occupants (Figure 6b), the upward thermal plumes and the downward airflow close to the walls with a velocity of about 0.5 m/s. There were some vortices in this cross-section. Comparing Figures 3 and 4, the inlet velocity (or ACH) dramatically affected the airflow pattern in this diffuser setup.

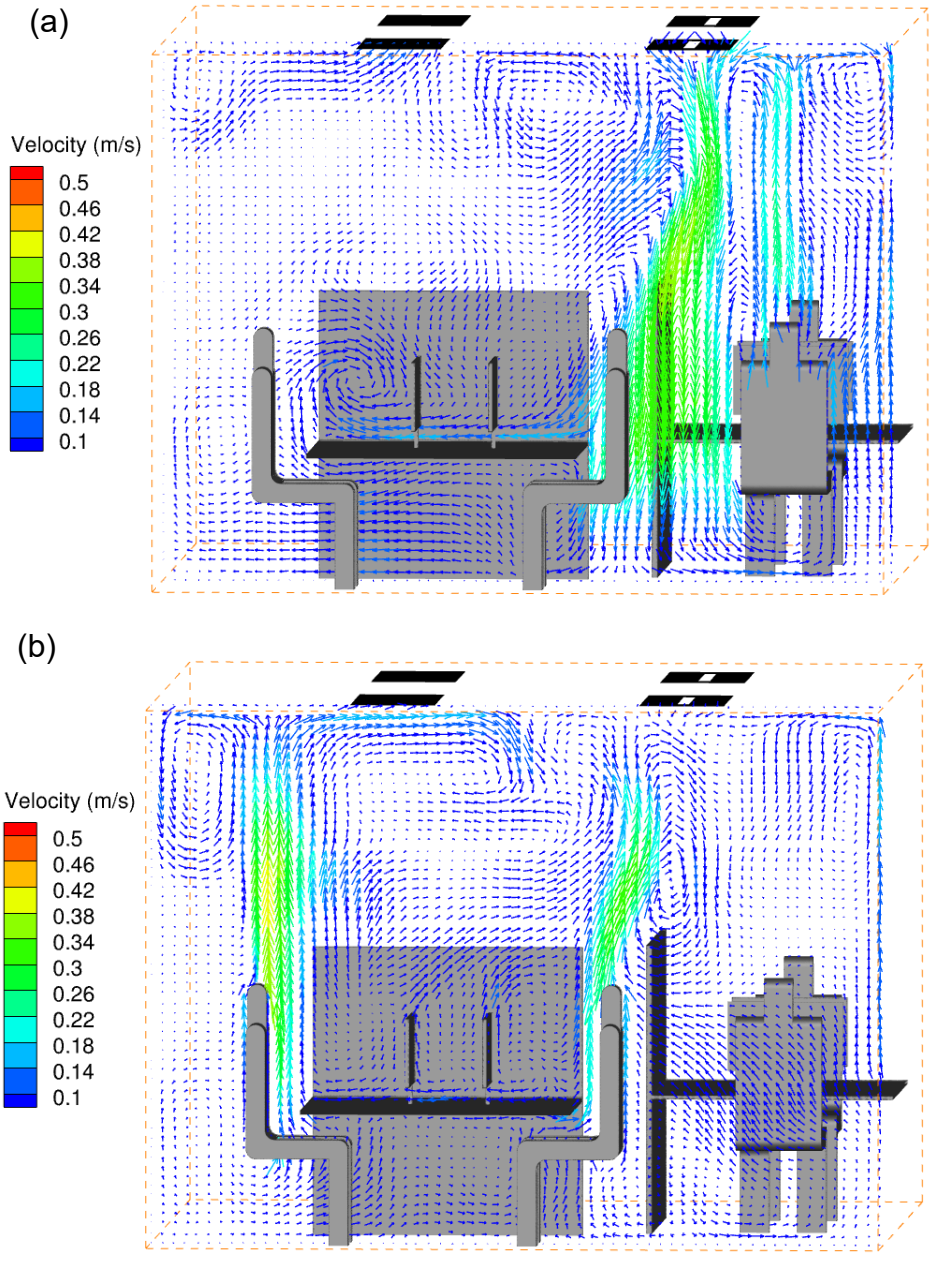

Figure 5. Airflow field in the x-axis cross sections (a) passing through the inlet diffuser X-1 cut and (b) passing through the human users X-2 cut, for geometric setup 1 and an ACH of 4 with an inlet velocity of 0.1 m/s.

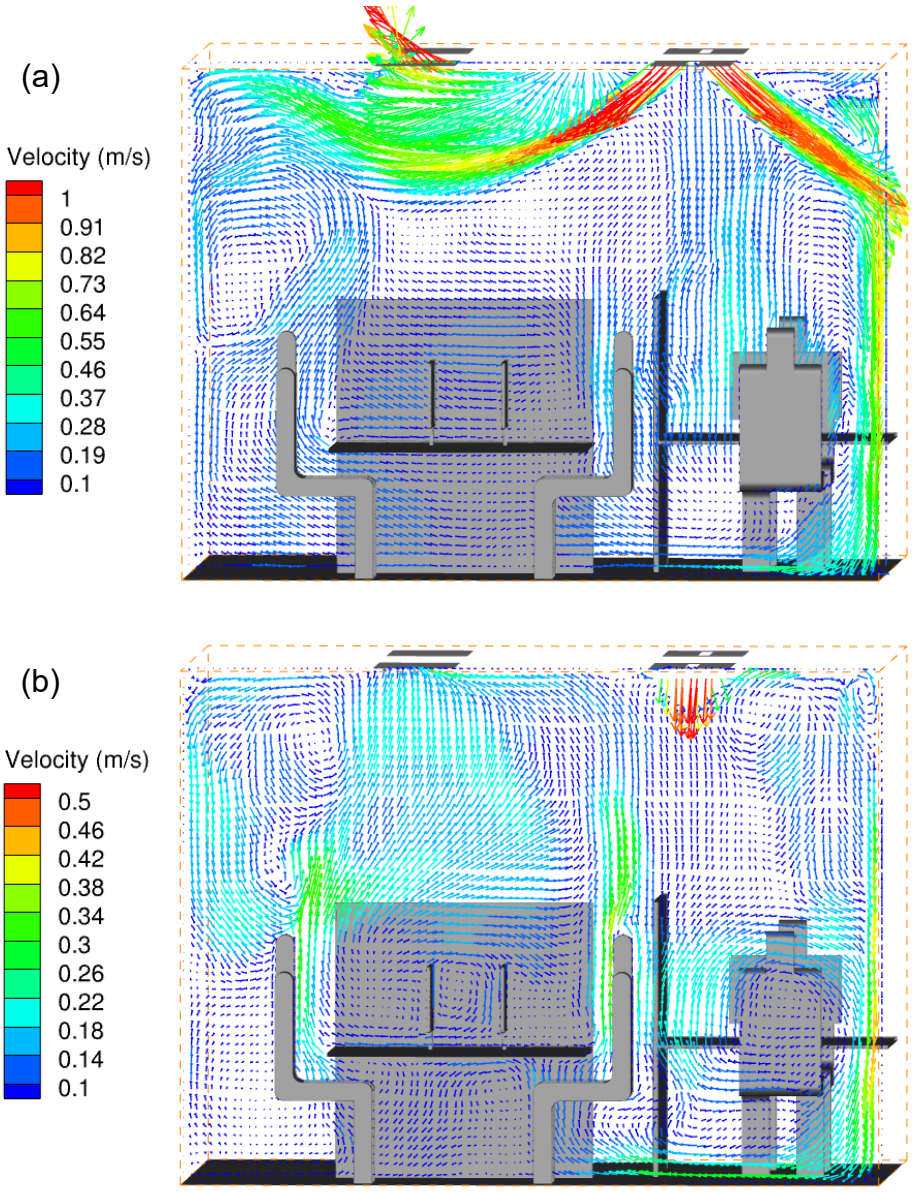

Figure 6. Airflow field in the x-axis cross sections (a) passing through the inlet diffuser X-1 cut and (b) passing through the human users X-2 cut, for geometric setup 1 and an ACH of 40 with an inlet velocity of 1 m/s.

Figure 7 shows the temperature contours in two x-axis cross sections for geometric setup 1 and an ACH of 4 with an inlet velocity of 0.1 m/s. For the cross-section passing the inlet (Figure 7a), the cool air impinged on the ground, which had a lower temperature than the surroundings. The temperature at the lower part of the office was 24-25°C, and the upper part was approximately 26° C. For the cross-section passing the human occupant (Figure 7b), the vertical direction temperature distribution was similar to Figure 7a. The lower and upper parts had a temperature of approximately 24-25ºC and 26°C, respectively. The human occupants generated upward thermal plumes with a temperature of around 26-27ºC. Combined with the thermal plumes from the monitors on the desk, a relatively warmer area between the two human occupants was formed in comparison to the surroundings.

Figure 8 shows the temperature contours in two x-axis cross sections for geometric setup 1 and an ACH of 40 with an inlet velocity of 1 m/s. For the cross-section passing through the inlet (Figure 8a), the cool air was delivered into the office with an angle of 45° due to the higher inlet velocity than in the case of ACH 4. The cool air was then sent to the near-wall regions with a temperature of 20-21°C. The inner region of the office had a higher temperature of 21-22°C. For the cross-section passing through the office occupants (Figure 8b), the inner region was warmer than the surrounding near-wall region. The upward thermal plumes had a temperature of around 22°C. The indoor temperature of the office under ACH 40 was around 3°C lower than that of ACH 4, as shown in Figure 8a.

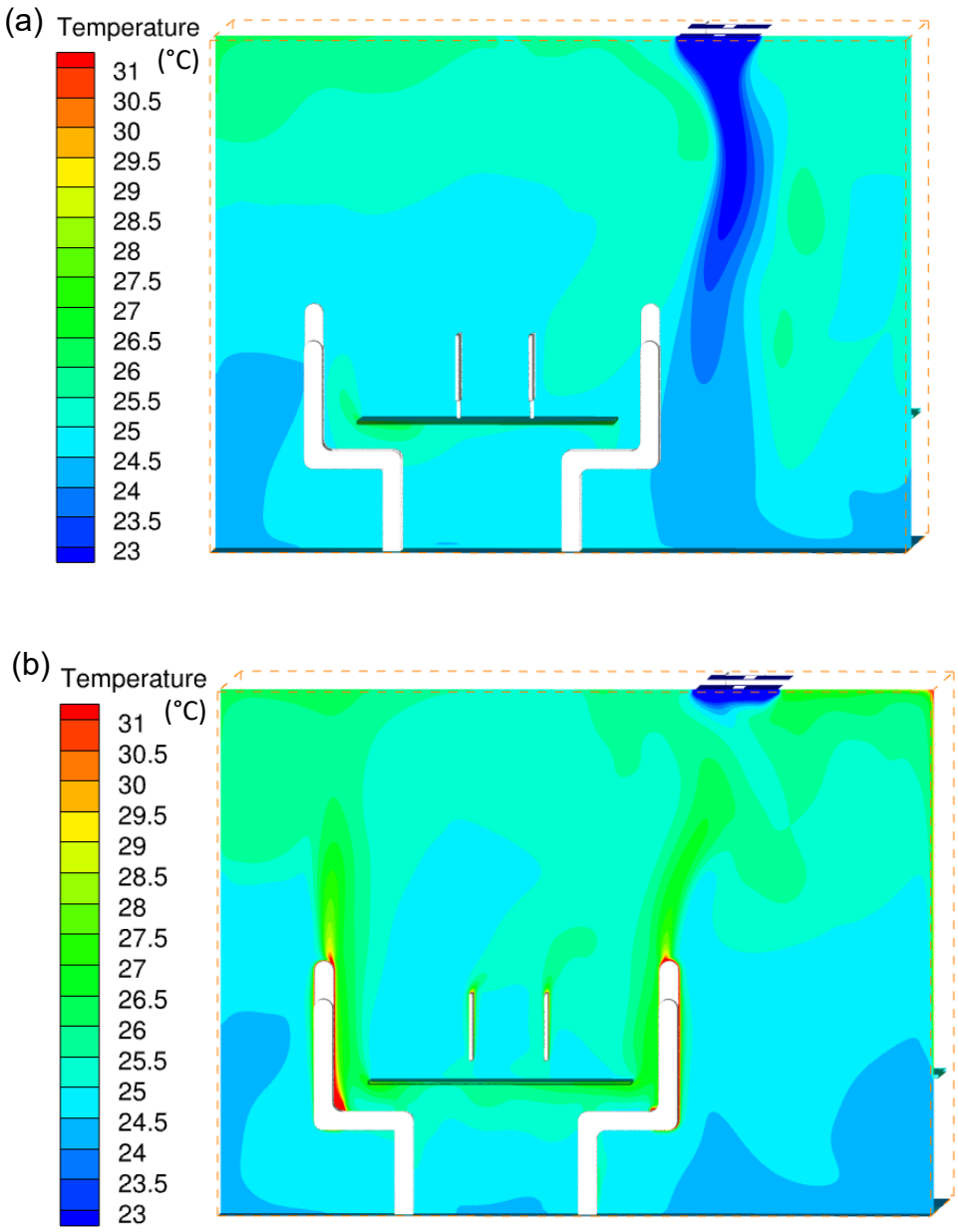

Figure 7. Temperature contour in the x-axis cross sections (a) passing through the inlet diffuser X-1 cut and (b) passing through the human users X-2 cut, for geometric setup 1 and an ACH of 4 with an inlet velocity of 0.1 m/s.

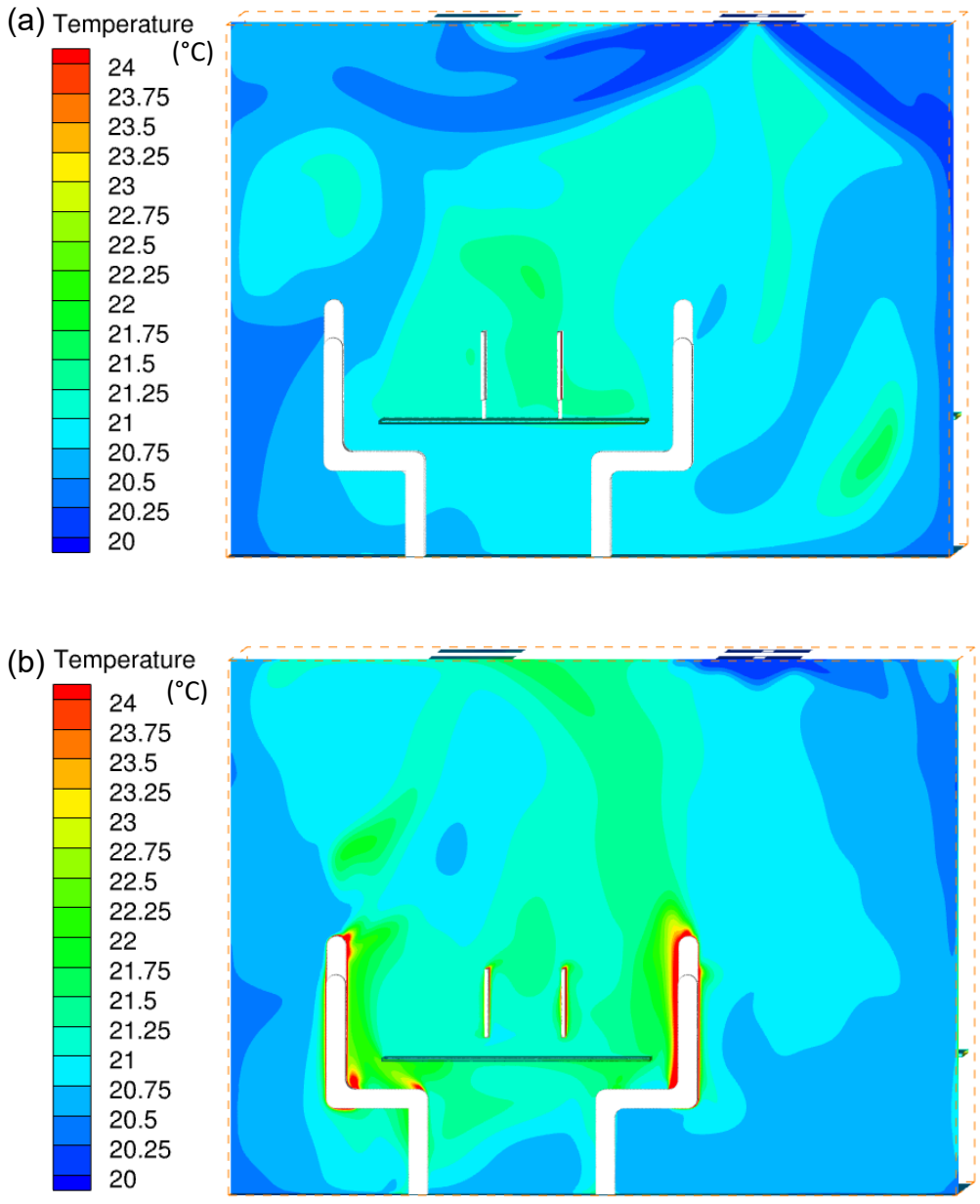

Figure 8. Temperature contour in the x-axis cross sections (a) passing through the inlet diffuser X-1 cut and (b) passing through the human users X-2 cut, for geometric setup 1 and an ACH of 40 with an inlet velocity of 1 m/s.

Intake fractions of different users to individual LCD

The exposure intake fractions of occupants to different LCD monitors with geometric setup 1 are shown in Figure 9. For ACH of 4, the human occupants were exposed to all four LCD monitor sources with a similar magnitude of the intake fraction (i.e. (1-2) × 10^{-3} per LCD) from each LCD. This is due to the mixing situation created by the large-scale flipping. With increasing ACH, the deviation of the intake fraction of each user from a single LCD source became more prominent due to the larger central circulation in the office. In addition, the increase in ACH significantly reduced the exposure intake fractions of the human occupants to the scale of 10^{-4}, because the VOC molecules were more effectively exhausted from the office under larger ACHs.

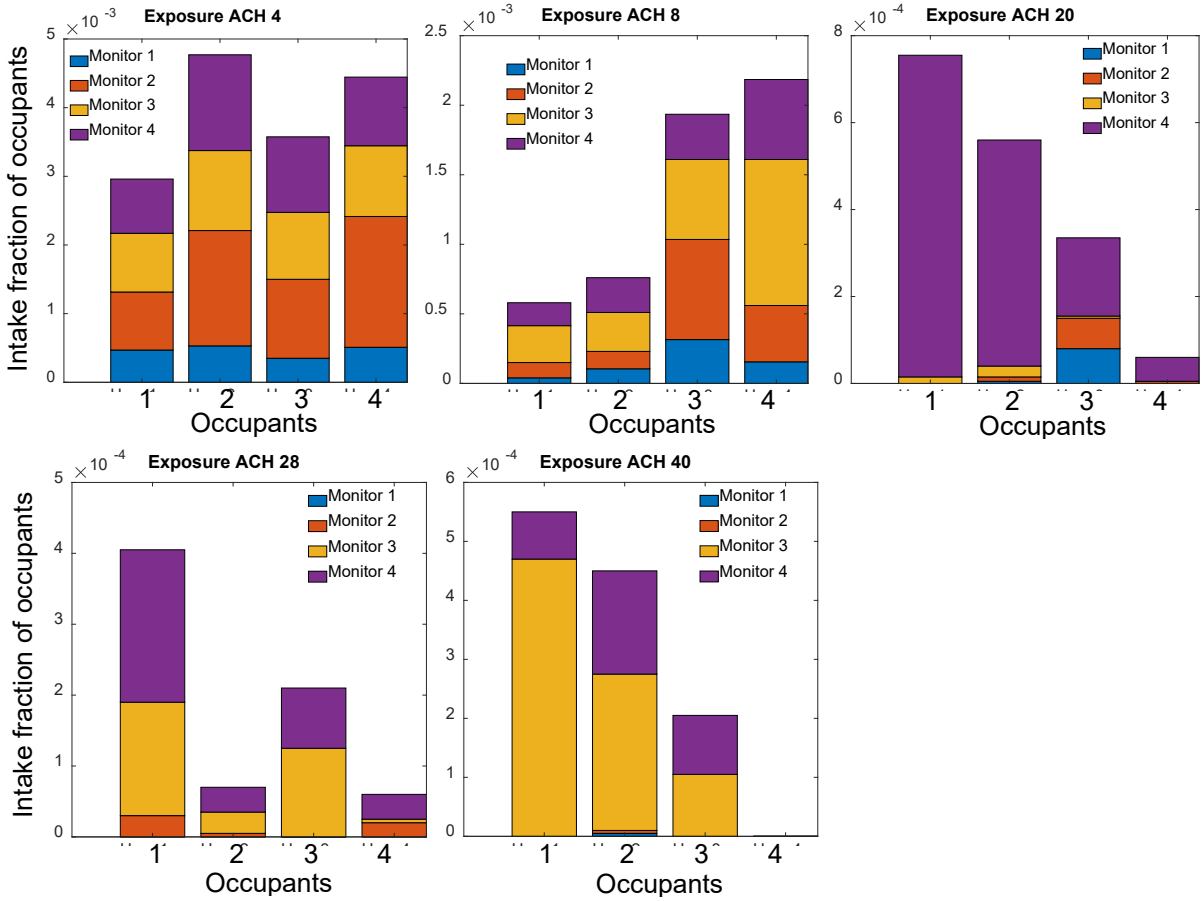

Figure 9. Exposure intake fractions of human occupants to individual LCD monitor sources under different ACHs in geometric setup 1 with partitioning.

The exposure intake fractions of occupants to each LCD source in geometric setup 1 without partitions were shown in Figure 10. As the ACH was increased to 40, the intake fractions was gradually reduced from 10^{-3} to 10^{-4}. Under the ACH of 4 and 8, the intake fractions from the four monitors were similar. For the ACH of 20, 28 and 40, the intake fractions from monitor 3 were much higher than the other monitors. Under each ACH, the intake fractions without partitions were at the same magnitude as those with partitions.

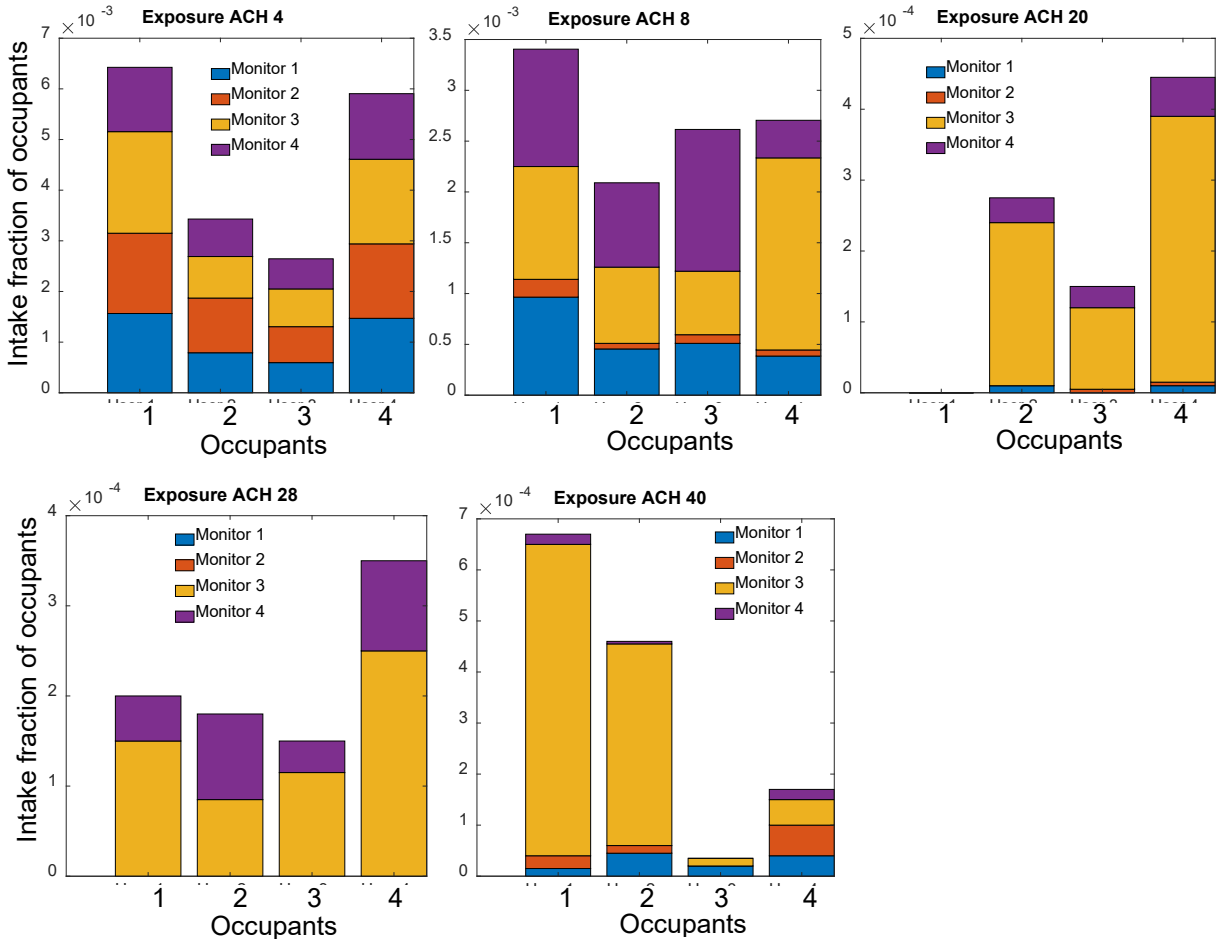

Figure 10. Exposure intake fractions of human occupants to individual LCD monitor sources under different ACHs in geometric setup 1 without partitioning

Effect of ACH on intake fraction of VOC molecules

Box plot was drawn to evaluate the overall intake fractions relative to ACH for each case, as shown in Figure 11a. For ACH of 4, the intake fractions in the office were in the range of (0.7-2.5) × 10^{-3}, with a median of approximately 1.5 × 10^{-3}. As ACH was increased to 8 and 20, the intake fractions were decreased almost linearly to approximately 0.7 × 10^{-3} and 0.2 × 10^{-3}, respectively (Figure 9a), and the reduction ratio of intake fractions compared to ACH of 4 was about 51% and 88% respectively (Figure 11b). When ACH was further increased to 40, the intake fractions were slightly reduced to 0.1 × 10^{-3}, and the reduction ratios were further increased to 92% and 93%, respectively. For individual geometric setups and partitions, the detailed intake fractions had the same variation trend as ACH. An ACH of 8-20 is recommended to achieve a cost-effective balance in the office environment.

Furthermore, for ACH of 4, the maximum intake fraction in the office was about four times the minimum value. For ACH of 8, the maximum-to-minimum ratio was as high as 9. For higher ACHs, the ratio was even higher. This suggested the significant spatial deviation of human exposure in different areas and geometric setups.

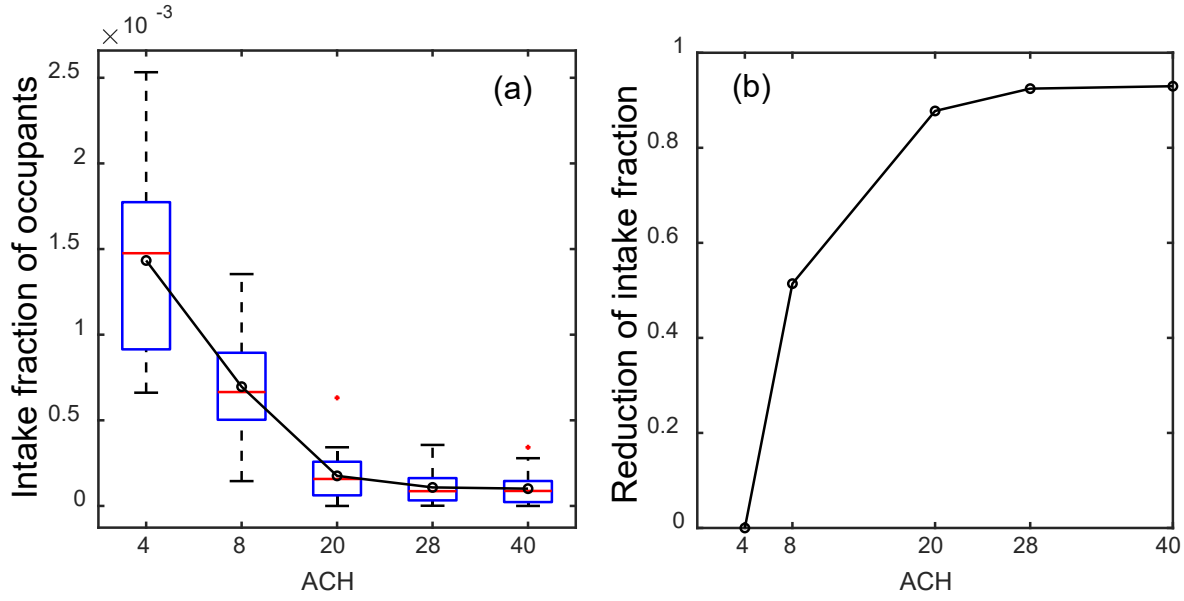

Figure 11. Effect of ACH on the exposure intake fraction of occupants in the office. (a) Intake fractions with increasing ACHs. The data for each ACH contain four geometric setups with and without partitioning. The black circles are the mean values of each ACH. (b) The reduction ratio of intake fraction with increasing ACHs was compared to ACH of 4.

Effect of geometric setup on intake fraction of VOC molecules

The intake fractions under various geometric setups are shown in Figure 12. For the cases with partitions, for all the study ACHs, setup 1 produced the most minor intake fractions, while setup 4 produced the highest intake fraction. For ACHs of 8-40, setups 1 and 3 produced relatively more minor intake fractions, while setups 2 and 4 produced higher intake fractions. For different ACHs, the median value for setup 4 was about 2-3 times that of setup 1, indicating the importance of geometric setups for human exposure.

For the cases without partitions, the geometric setup 1 produced relatively more minor intake fractions than other setups. The differences between the different setups were not significant. The ratio of the medians of the different setups was about 1-2 times. The higher the ACH, the smaller the intake fractions of the different geometric setups.

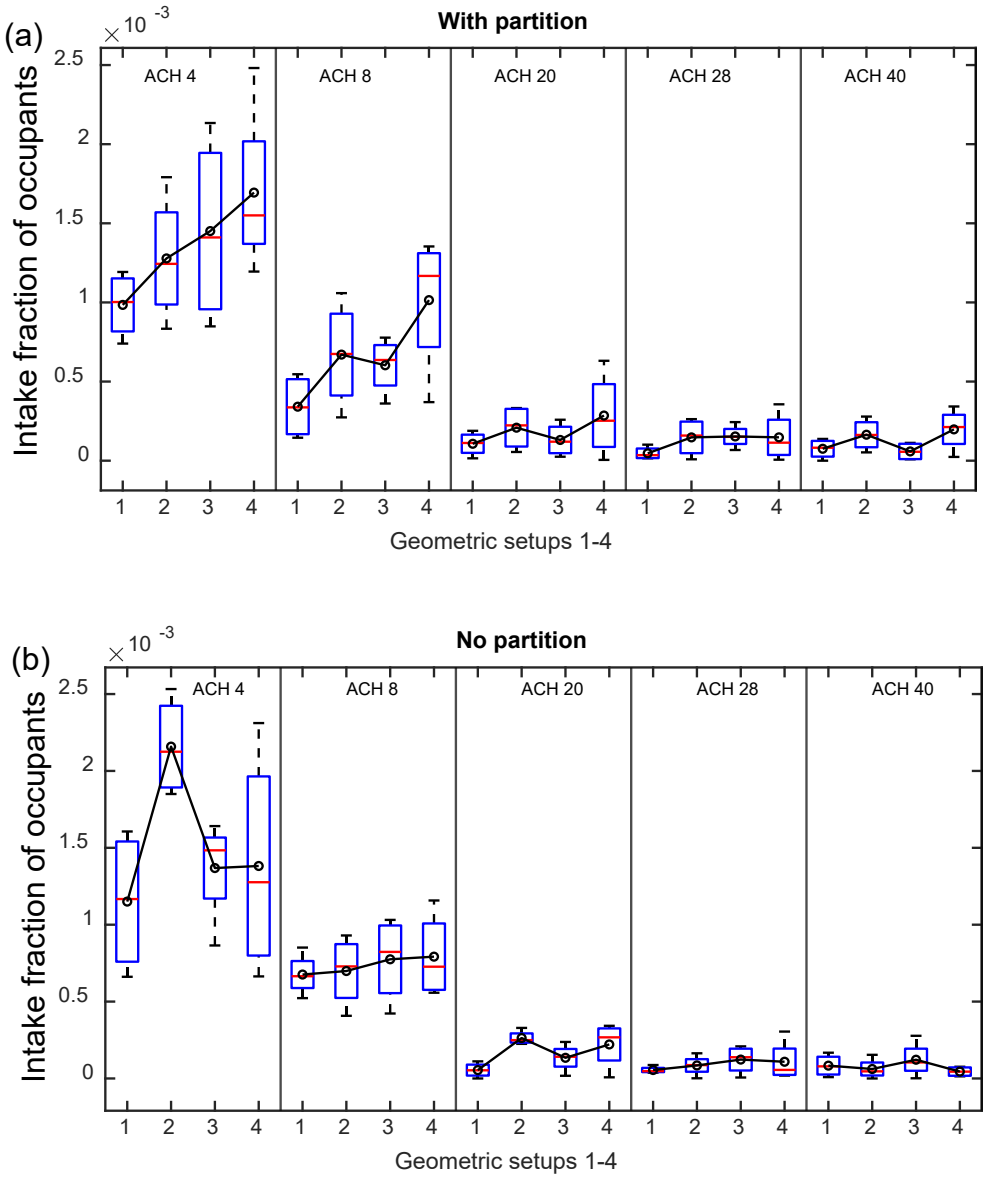

Figure 12. Exposure intake fractions for the four geometric setups 1-4 (a) with partitioning and (b) without partitioning. The black circles are the mean values for each setup.

The effect of the physical partitioning on the exposure intake fractions of VOC molecules

Figure 13 shows the effect of partitioning on the exposure intake fractions in various cases. For setups 1, 2 and 3, for smaller ACHs, the intake fraction for the case without partition was higher than that for the case with partition. For setup 4, the intake fraction for the case without

partition was smaller for smaller ACHs. While for higher ACH of 20, 28 and 40, the intake fraction for most cases without partitions was smaller. This was because partitioning can create semi-enclosed areas. For higher ACHs, ventilation can remove VOC molecules more effectively without partitions.

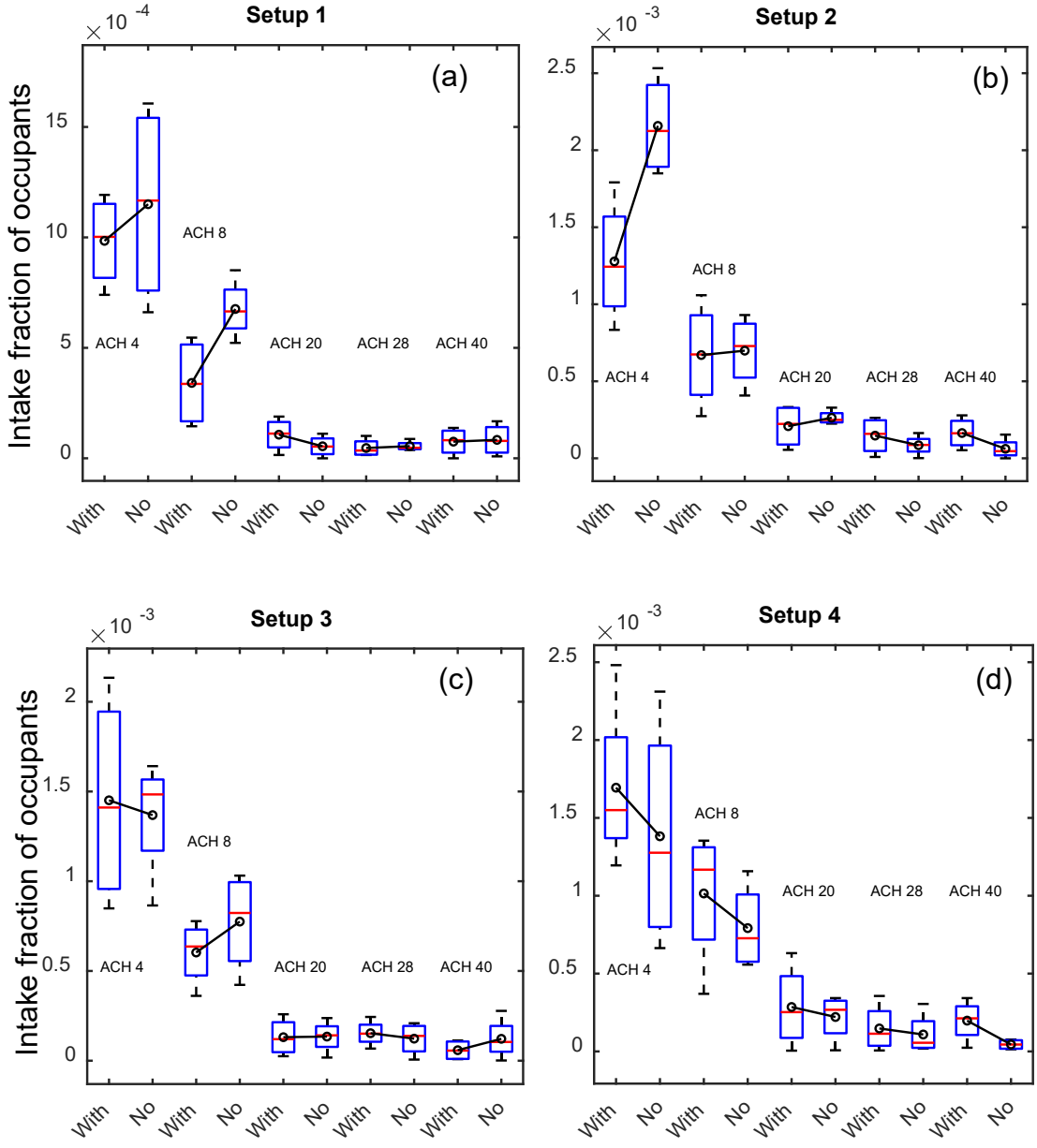

Figure 13. The effect of partitioning on the intake fraction. (a-d) Geometric setups 1-4. The black circles are the mean values of intake fractions. "With" indicated the cases with partitioning. "No" indicated the cases in which no partitioning on the desk.

Lifetime exposure to VOC molecules from each LCD source in the office

The inhaled number and mass doses over a lifetime (30 years) are shown in Figure 14. For ACH of 4, the inhaled number dose over the lifetime was about 8.2×10^{18}. When ACH was increased to 20, the number dose was decreased to about 1.0×10^{18}, and there was no further reduction in dose with further increase in ACH. The corresponding mass exposure during 30 years of office work was in the range of 0.1 - 1 mg.

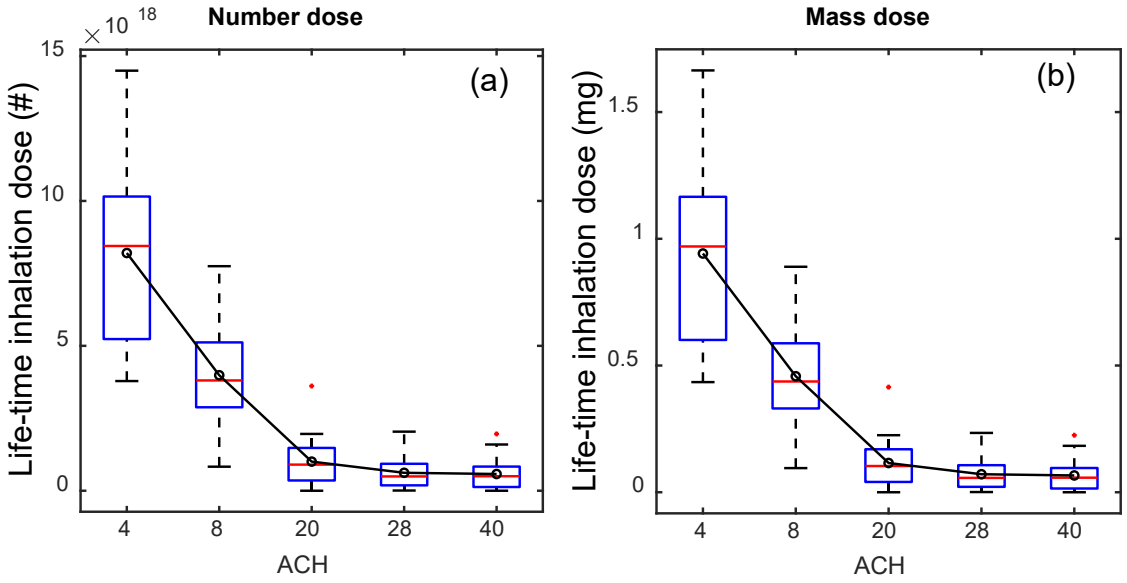

Figure 14. Lifetime exposure dose of human occupants in the office. (a) Number exposure dose and (b) mass exposure dose via inhalation. The black circles are the average values for each ACH.

Discussion

The LCD screens can emit more than 30 types of VOCs with a total emission rate of 8.25 × 10^9 molecules·s^{-1}·cm^{-2} at 23°C and 58% relative humidity, i.e., 3.3 μg·$hour^{-1}$·unit $screen^{-1}$.[20] The dominant VOCs are acetic acid, isoprene, cyclohexene, nonanal and 1,9-nonanediol with emission rates of 0.5 - 3 × 10^9 molecules·s^{-1}·cm^{-2}. The VOC emission from LCDs is significantly lower than the traditional indoor sources, such as hardboard and wood furniture, with emission of > 10 mg·h^{-1}·$unit^{-1}$ as indicated in previous studies.[50, 51] However, people spend most of their time indoors and are increasingly exposed to modern LCD screens with a shorter distance than traditional carpet or wood products. The emission of LCD VOCs indoors raises a new concern about the adverse health effects in indoor environments, although the emission rate is lower than that of traditional building sources. The intake fraction and lifetime exposure to the LCD VOCs were investigated in this work.

The results of this work revealed exposure of office occupants to LCD VOC molecules and indicated that exposure was affected by user location, ventilation rate and geometric setup. Lifetime exposure via inhalation was approximately 8.2 × 10^{18} molecules. Higher ACH could reduce exposure by approximately 88%, which is about one order of magnitude reduction. Increasing ACH could effectively reduce the exposure, and the optimal ACH was recommended to be 20 to achieve a cost-effective balance. A proper geometric setting design could achieve a 2-3 times reduction compared to a poor setting, including desk location, orientation and partitions. Different locations of office occupants could lead to a 4 - 9 times deviation in exposure to VOC molecules. The ratio might vary to some extent, considering the instability of ventilation flow rate, which was not considered in this study. The results indicated that enhancing ventilation rate could significantly reduce human exposure to indoor VOCs, but it could also increase energy consumption. A proper geometric setting would achieve a moderate exposure reduction without

increasing energy consumption, which requires specific design and consideration of ventilation type.

To evaluate VOC concentrations, the lifetime inhalation exposure of 8.2×10^{18} molecules or 1 mg per LCD was converted to VOC concentration using a pulmonary rate of 0.84 m^3/h,[39] lifetime duration and approximately 2.62 $\mu g/m^3$ per ppb.[52] After conversion to concentration, the VOC concentration of the inhaled air was equivalent to 5.2×10^{-3} ppb, which is much lower than the approximately 5.6×10^2 ppb exposure of LCD industry workers.[23-25] However, the above analysis was based on the emission rate of 8.25×10^9 molecules$\cdot s^{-1} \cdot cm^{-2}$ and four desk-based LCD screens at the temperature 23°C and 58% relative humidity in a well-ventilated staff office. Higher temperatures or moisture can enhance the VOC emission rate a few times from different indoor materials. [53-55] In addition, the large offices for students or staff may have up to tens of LCD screens and personal electronic devices, which would release much more VOCs than the studied office and could lead to higher lifetime exposure. The exposure would be even higher when the indoor environments are less ventilated than the ASHRAE standard of 2 - 4 ACH.[35, 56] Exposure to LCD VOCs should be a new concern in indoor environments.

There are many indoor VOC sources, including furniture, decoration and cleaning products. Exposure to VOCs in indoor environments is of particular concern for health reasons. Considering mixed ventilation in commercial buildings, the intake fractions in this work (i.e., $0.7\text{-}2.5 \times 10^{-3}$) can be extended to other indoor VOC sources, such as desks, cabinets and carpets in new offices, together with the corresponding emission rates.[57-59] This work only evaluated exposure to a recently discovered source of VOCs from LCD monitors in office environments through computational fluid dynamics simulations. Further studies could simultaneously consider other indoor VOC sources, such as desks, carpets, decorations and cleaning products. Indoor VOC

concentrations and exposure could be estimated through numerical simulations and compared with field measurements.

There are some limitations in this study. First, human exposure to VOC molecules can be divided into three categories: ingestion, dermal contact and inhalation.[38, 60-64] This study mainly focused on the exposure to VOCs via the inhalation. In the future, exposure via ingestion and dermal contact can be added to the numerical modelling. Second, this study did not consider the chemical reaction of VOCs in the office. For the offices facing outside, the intense sun radiation may induce photochemical reactions and release new contaminants such as secondary aerosols.[65, 66] Third, we take a small four-person office as an example for exposure analysis in this work. The exposure may show different features in a much larger office with more LCD monitors, such as student offices and commercial buildings. Finally, this work studied the LCD VOC exposure under mixing ventilation with typical office diffusers. There are different types of ventilation, such as mixing, impingement and displacement. Different ventilation types have various contaminant removal abilities, as indicated by previous studies for airborne particles.[67, 68] More studies are necessary to fully evaluate VOC exposure in indoor environments.

Conclusion

This is the first study to evaluate the dispersion of LCD VOCs and the lifetime exposure in offices. An experimentally validated numerical simulation was employed to evaluate the ratio of inhaled VOC molecules to LCD emissions. The lifetime exposure to LCD VOCs under various ACHs, geometric settings and partitions was also evaluated. The following conclusions were drawn from this study:

(1) Under various office scenarios with an ACH of 4, the range of intake fractions in the office was 0.7-2.5 × 10^{-3}, with a median of 1.5 × 10^{-3}, which is within the ASHRAE recommended ACH range of 2-4 for offices.

(2) As ACH was increased to 20, the median intake fraction can be linearly reduced to about 0.17 × 10^{-3}, with a reduction rate of about 88%. However, the intake fraction can only be slightly reduced when ACH was further increased to 40.

(3) When ACH was 4 - 8, the exposure deviation of occupants in different locations can reach 4 - 9 times. The higher the ACH, the more obvious the deviation.

(4) The intake fraction also depends on the geometric setting and partition. The worst geometric setting was about 2 - 3 times the proper geometry. Geometric settings 1 and 3 with partitions were recommended for offices.

(5) For a normal ACH of 4, the lifetime exposure dose per LCD source was about 8.2 × 10^{18} molecules, corresponding to a mass exposure dose of 1 mg in 30 years of office work.

(6) The results of this work indicated that exposure to VOCs from LCD screens was well below acceptable levels in the well-ventilated office at 23°C and 58% relative humidity. However, the exposure to LCD VOCs would be higher under warmer and humid conditions because of the enhanced emission. The indoor exposure would be more complicated and should be a new concern, considering the potential chemical reactions with the VOCs from other indoor sources.

This work provides a fundamental understanding of the dispersion and exposure to VOC molecules from LCD in office environments.

Acknowledgments

This research was supported by the Collaborative Research Fund (CRF) Scheme (C5024-21G) of the Research Grants Council of the Hong Kong Special Administrative Region and the RAP Start-up Fund under the Strategic Hiring Scheme (A0043523) of The Hong Kong Polytechnic University.

Author Contribution

All authors contributed equally in the preparation of this manuscript.

Declaration of competing interest

The authors have no competing interests to declare that are relevant to the content of this article.

References

1. Gligorovski S and Abbatt JP. An indoor chemical cocktail. *Science* 2018; 359: 632-633.

2. Weschler CJ and Carslaw N. Indoor chemistry. *Environ Sci Technol* 2018; 52: 2419-2428.

3. Goldstein AH, Nazaroff WW, Weschler CJ and Williams J. How do indoor environments affect air pollution exposure? *Environ Sci Technol* 2020; 55: 100-108.

4. Spengler JD and Sexton K. Indoor air pollution: a public health perspective. *Science* 1983; 221: 9-17.

5. Zhang J and Smith KR. Indoor air pollution: a global health concern. *Brit Med Bull* 2003; 68: 209-225.

6. Azuma K, Uchiyama I and Ikeda K. The regulations for indoor air pollution in Japan: a public health perspective. *J Risk Res* 2008; 11: 301-314.

7. Guo H, Lee SC, Chan L and Li W. Risk assessment of exposure to volatile organic compounds in different indoor environments. *Environ Res* 2004; 94: 57-66.

8. Liu N, Bu Z, Liu W, Kan H, Zhao Z, Deng F, Huang C, Zhao B, Zeng X and Sun Y. Health effects of exposure to indoor volatile organic compounds from 1980 to 2017: a systematic review and meta-analysis. *Indoor Air* 2022; 32: e13038.

9. Yoon H-I, Hong Y-C, Cho S-H, Kim H, Kim YH, Sohn JR, Kwon M, Park S-H, Cho M-H and Cheong H-K. Exposure to volatile organic compounds and loss of pulmonary function in the elderly. *Eur Respir J* 2010; 36: 1270-1276.

10. Ma C-M, Lin L-Y, Chen H-W, Huang L-C, Li J-F and Chuang K-J. Volatile organic compounds exposure and cardiovascular effects in hair salons. *Occup Med* 2010; 60: 624-630.

11. Kwon J-W, Park H-W, Kim WJ, Kim M-G and Lee S-J. Exposure to volatile organic compounds and airway inflammation. *Environ Health* 2018; 17: 1-8.

12. Sonne C, Xia C, Dadvand P, Targino AC and Lam SS. Indoor volatile and semi-volatile organic toxic compounds: Need for global action. *J Build Eng* 2022; 62: 105344.

13. You B, Zhou W, Li J, Li Z and Sun Y. A review of indoor gaseous organic compounds and human chemical exposure: insights from real-time measurements. *Environ Int* 2022; 170: 107611.

14. Liu Y, Misztal PK, Xiong J, Tian Y, Arata C, Weber RJ, Nazaroff WW and Goldstein AH. Characterizing sources and emissions of volatile organic compounds in a northern California residence using space-and time-resolved measurements. *Indoor Air* 2019; 29: 630-644.

15. Hernandez G, Wallis SL, Graves I, Narain S, Birchmore R and Berry T-A. The effect of ventilation on volatile organic compounds produced by new furnishings in residential buildings. *Atmos Environ: X* 2020; 6: 100069.

16. McDonald BC, De Gouw JA, Gilman JB, Jathar SH, Akherati A, Cappa CD, Jimenez JL, Lee-Taylor J, Hayes PL and McKeen SA. Volatile chemical products emerging as largest petrochemical source of urban organic emissions. *Science* 2018; 359: 760-764.

17. Uhde E and Schulz N. Impact of room fragrance products on indoor air quality. *Atmos Environ* 2015; 106: 492-502.

18. Nazaroff WW and Weschler CJ. Cleaning products and air fresheners: exposure to primary and secondary air pollutants. *Atmos Environ* 2004; 38: 2841-2865.

19. Klein F, Farren NJ, Bozzetti C, Daellenbach KR, Kilic D, Kumar NK, Pieber SM, Slowik JG, Tuthill RN and Hamilton JF. Indoor terpene emissions from cooking with herbs and pepper and their secondary organic aerosol production potential. *Sci Rep* 2016; 6: 36623.

20. Liu Q and Abbatt JP. Liquid crystal display screens as a source for indoor volatile organic compounds. *Proc Natl Acad Sci USA* 2021; 118: e2105067118.

21. Markit I. Large TFT LCD panel shipments increased in 2018 despite market concerns, https://news.ihsmarkit.com/prviewer/release_only/slug/technology-large-tft-lcd-panel-shipments-increased-2018-despite-market-concernsihs-ma (2019). Accessed 4 March 2024.

22. Research O. Global liquid crystal monomer market analysis 2015-2019 and forecast 2020-2025, https://www.orbisresearch.com/reports/index/global-liquid-crystal-monomer-market-analysis-2013-2018-and-forecast-2019-2024 (2019). Accessed 6 March 2024.

23. Chang T-Y, Huang K-H, Liu C-S, Shie R-H, Chao K-P, Hsu W-H and Bao B-Y. Exposure to volatile organic compounds and kidney dysfunction in thin film transistor liquid crystal display (TFT-LCD) workers. *J Hazard Mater* 2010; 178: 934-940.

24. Chang T-Y, Huang K-H, Liu C-S and Bao B-Y. Exposure to indoor volatile organic compounds and hypertension among thin film transistor liquid crystal display workers. *Atmosphere* 2020; 11: 718.

25. Wang Y-F, Wang S-M, Kuo Y-C, Yoon C, Wang Y-F and Tsai P-J. Long-term multiple chemical exposure assessment for a thin film transistor liquid crystal display (TFT-LCD) industry. *Aerosol Air Qual Res* 2017; 17: 2891-2900.

26. Fu Y, Lin X, Zheng X, Wang L, Liu C-H, Zhang X, Li CY and Tse K. Physio-chemical modeling of the NO_x-O_3 photochemical cycle and the air pollutants' reactive dispersion around an isolated building. *Build Simul* 2023; 16(9): 1735-1758.

27. Yang X, Srebric J, Li X and He G. Performance of three air distribution systems in VOC removal from an area source. *Build Environ* 2004; 39: 1289-1299.

28. Deng B and Kim CN. CFD simulation of VOCs concentrations in a resident building with new carpet under different ventilation strategies. *Build Environ* 2007; 42: 297-303.

29. Zhang Q and Zhang G. Study on TVOCs concentration distribution and evaluation of inhaled air quality under a re-circulated ventilation system. *Build Environ* 2007; 42: 1110-1118.

30. Tong Z and Liu H. Modeling in-vehicle VOCs distribution from cabin interior surfaces under solar radiation. *Sustainability* 2020; 12: 5526.

31. Zhao L, Zhou H, Jin Y and Li Z. Experimental and numerical investigation of TVOC concentrations and ventilation dilution in enclosed train cabin. *Buildi Simul* 2022;15(5): 1-14.

32. Wang C, Fu S and Chao CY. Short-range bioaerosol deposition and recovery of viable viruses and bacteria on surfaces from a cough and implications for respiratory disease transmission. *Aerosol Sci Technol* 2021; 55: 215-230.

33. Wang C, Xu J, Chan K, Lee H, Tso C, Lin CS, Chao CY and Fu S. Infection control measures for public transportation derived from the flow dynamics of obstructed cough jet. *J Aerosol Sci* 2022; 163: 105995.

34. Wang C, Xu J, Fu S and Chao CY. Airborne infection risk of nearby passengers in a cabin environment and implications for infection control. *Travel Med Infect Di* 2022; 47: 102285.

35. *ASHRAE Handbook — HVAC Applications*. Atlanta: ASHRAE, 2023.

36. Li H, Zhong K and Zhai ZJ. Investigating the influences of ventilation on the fate of particles generated by patient and medical staff in operating room. *Build Environ* 2020; 180: 107038.

37. Sun C and Zhai Z. The efficacy of social distance and ventilation effectiveness in preventing COVID-19 transmission. *Sustain Cities Soc* 2020; 62: 102390.

38. Fridman I. Surface Area of Human Skin, https://hypertextbook.com/facts/2001/IgorFridman.shtml (2001). Accessed 10 March 2024.

39. Gupta JK, Lin CH and Chen Q. Characterizing exhaled airflow from breathing and talking. *Indoor Air* 2010; 20: 31-39.

40. Katramiz E, Ghaddar N, Ghali K, Al-Assaad D and Ghani S. Effect of individually controlled personalized ventilation on cross-contamination due to respiratory activities. *Build Environ* 2021; 194: 107719.

41. Xu J, Wang C and Guo H. Effect of personalized air curtain combined with mixing ventilation on dispersion of aerosols released at different velocities from respiratory activities during close contact. *J Build Eng* 2024: 87: 109016.

42. Georgescu MR, Meslem A, Nastase I and Bode F. Personalized ventilation solutions for reducing CO2 levels in the crew quarters of the International Space Station. *Build Environ* 2021; 204: 108150.

43. Lv L, Wu Y, Cao C, Zeng L, Gao J, Xie W and Zhang J. Impact of different human walking patterns on flow and contaminant dispersion in residential kitchens: Dynamic simulation study. *Build Simul* 2022;15(6): 1-16.

44. Yan W, Zhang Y, Sun Y and Li D. Experimental and CFD study of unsteady airborne pollutant transport within an aircraft cabin mock-up. *Build Environ* 2009; 44: 34-43.

45. Stabile L, Pacitto A, Mikszewski A, Morawska L and Buonanno G. Ventilation procedures to minimize the airborne transmission of viruses in classrooms. *Build Environ* 2021; 202: 108042.

46. Gilkeson C, Camargo-Valero M, Pickin L and Noakes C. Measurement of ventilation and airborne infection risk in large naturally ventilated hospital wards. *Build Environ* 2013; 65: 35-48.

47. Qin C, Zhang S-Z, Li Z-T, Wen C-Y and Lu W-Z. Transmission mitigation of COVID-19: Exhaled contaminants removal and energy saving in densely occupied space by impinging jet ventilation. *Build Environ* 2023; 232: 110066.

48. Xu Y, Yang X, Yang C and Srebric J. Contaminant dispersion with personal displacement ventilation, Part I: Base case study. *Build Environ* 2009; 44: 2121-2128.

49. Inc. A. *13.2.4 Natural Convection and Buoyancy-Driven Flows*. https://www.afs.enea.it/project/neptunius/docs/fluent/html/ug/node470.htm (2009). Accessed 10 March 2024.

50. Brown S. Chamber assessment of formaldehyde and VOC emissions from wood-based panels. *Indoor Air* 1999; 9: 209-215.

51. Guo H, Murray F and Lee S-C. Emissions of total volatile organic compounds from pressed wood products in an environmental chamber. *Build Environ* 2002; 37: 1117-1126.

52. Technologies B. Air pollution – How to convert between mg/m^3, µg/m^3 and ppm, ppb, https://www.breeze-technologies.de/blog/air-pollution-how-to-convert-between-mgm3-%C2%B5gm3-ppm-ppb/ (2021). Accessed 10 March 2024.

53. Zhou S, Liu H, Ding Y and Wu Y. The effects of temperature and humidity on the VOC emission rate from dry building materials. *IOP Conference Series: Mat Sci Eng* 2019; Vol???: 042001.

54. Beel G, Langford B, Carslaw N, Shaw D and Cowan N. Temperature driven variations in VOC emissions from plastic products and their fate indoors: A chamber experiment and modelling study. *Sci Total Environ* 2023; 881: 163497.

55. Zhu Y, Guo S and Liang W. A literature review investigating the impact of temperature and humidity on volatile organic compound emissions from building materials. *Build Environ* 2024: 111845.

56. *ASHRAE Handbook-Fundamentals*. Atlanta: ASHRAE, 2021.

57. Tang X, Misztal PK, Nazaroff WW and Goldstein AH. Volatile organic compound emissions from humans indoors. *Environmental Science & Technology* 2016; 50: 12686-12694.

58. Gao M, Liu W, Wang H, Shao X, Shi A, An X, Li G and Nie L. Emission factors and characteristics of volatile organic compounds (VOCs) from adhesive application in indoor decoration in China. *Sci Total Environ* 2021; 779: 145169.

59. Huang L, Wei Y, Zhang L, Ma Z and Zhao W. Estimates of emission strengths of 43 VOCs in wintertime residential indoor environments, Beijing. *Sci Total Environ* 2021; 793: 148623.

60. Creta M, Poels K, Thoelen L, Vranckx K, Collaerts P, Jansen F, Vangeel M, Godderis L, Duca R-C and Vanoirbeek JA. A method to quantitatively assess dermal exposure to volatile organic compounds. *Ann Work Expo Health* 2017; 61: 975-985.

61. Weschler CJ and Nazaroff WW. SVOC exposure indoors: fresh look at dermal pathways. *Indoor Air* 2012; 22: 356-377.

62. Roy A, Weisel C, Lioy P and Georgopoulos P. A distributed parameter physiologically-based pharmacokinetic model for dermal and inhalation exposure to volatile organic compounds. *Risk Anal* 1996; 16: 147-160.

63. Fan C, Wang G-S, Chen Y-C and Ko C-H. Risk assessment of exposure to volatile organic compounds in groundwater in Taiwan. *Sci Total Environ* 2009; 407: 2165-2174.

64. Cao F, Qin P, Lu S, He Q, Wu F, Sun H, Wang L and Li L. Measurement of volatile organic compounds and associated risk assessments through ingestion and dermal routes in Dongjiang Lake, China. *Ecotox Environ Safe* 2018; 165: 645-653.

65. Sbai SE, Li C, Boreave A, Charbonnel N, Perrier S, Vernoux P, Bentayeb F, George C and Gil S. Atmospheric photochemistry and secondary aerosol formation of urban air in Lyon, France. *J Environ Sci* 2021; 99: 311-323.

66. Xu J, Hu W, Liang D and Gao P. Photochemical impacts on the toxicity of PM2. 5. *Critical Reviews in Environ Sci Technol* 2022; 52: 130-156.

67. Li Y, Leung M, Tang J, Yang X, Chao CYH, Lin JZ, Lu J, Nielsen PV, Niu J and Qian H. Role of ventilation in airborne transmission of infectious agents in the built environment–a multidisciplinary systematic review. *Indoor Air* 2007; 17(1):2-18.

68. Fan M, Fu Z, Wang J, Wang Z, Suo H, Kong X and Li H. A review of different ventilation modes on thermal comfort, air quality and virus spread control. *Build Environ* 2022; 212: 108831.